JJMS **19**, No. 2, 181-201 (2026)

Jordan Journal of Mathematics and Statistics.
Yarmouk University

DOI:https://doi.org/10.47013/19.2.2

Approximate Solution Of Variable-Order Fractional Optimal Control Problems

Zahra Pirouzeh[1], *Kamele Nassiri Pirbazari*[2] *and Mohammad Hadi Noori Skandari*[3,*]

[1] Faculty of Mathematical Sciences, University of Guilan, Rasht, Iran
[2] Faculty of Mathematical Sciences, University of Guilan, Rasht, Iran
[3] Faculty of Mathematical Sciences, Shahrood University of Technology, Shahrood, Iran

Received: Nov. 4, 2024 Accepted: Dec. 1, 2025

Abstract: This paper introduces a robust and highly accurate numerical scheme for solving a general class of variable-order fractional optimal control (VOFOC) problems based on the Caputo definition. The proposed method leverages a shifted Legendre spectral collocation (SLSC) technique, which effectively combines the superior approximation properties of global polynomials with the precision of Gaussian quadrature. The core of our approach lies in the novel derivation of an operational matrix for the variable-order fractional derivative (VOFD) of shifted Legendre polynomials. This matrix allows for the exact representation of the VOFD of the state variable, thereby transforming the complex fractional dynamical system constraint into a computationally tractable system of algebraic equations. The state and control variables are approximated by finite expansions of shifted Legendre polynomials with unknown coefficients. The objective functional is discretized using the shifted Legendre-Gauss-Lobatto (SLGL) quadrature rule, which is exact for polynomials of sufficiently high degree. Consequently, the original continuous-time VOFOC problem is converted into a nonlinear programming (NLP) problem, which can be efficiently solved using standard optimization solvers. A rigorous convergence analysis is provided, establishing that under mild conditions, the sequence of approximate solutions generated by our method uniformly converges to the exact optimal solution of the original VOFOC problem. The efficacy, versatility, and superiority of the proposed framework are demonstrated through six comprehensive numerical examples, including a practical application to train motion control. Results show that our method achieves exponential convergence rates, outperforms existing techniques like the variational iteration method, wavelet methods, and other spectral schemes in terms of accuracy, and yields solutions very close to the exact ones even with a small number of basis functions. The method proves to be a powerful tool for handling the complexities inherent in variable-order fractional calculus, offering a blend of theoretical robustness and computational efficiency.

Keywords: Variable-order fractional derivatives; Variable-order fractional optimal control problems; Spectral-collocation method; Nonlinear programming.
2010 Mathematics Subject Classification. 26A25; 26A35.

1 Introduction

Physical and natural phenomena can be modeled more accurately using advanced mathematical tools such as fractional calculus, which provides greater precision than classical calculus approaches. In recent years, fractional calculus has made significant contributions across various fields including control theory, chemistry, biology, economics, and mechanics [1]-[5]. Particularly, fractional optimal control (FOC) problems involving fractional dynamical systems have attracted considerable research attention. Several researchers have explored necessary optimality conditions for FOC problems [6,11]. Lotfi et al. [18] transformed FOC problems into algebraic equation systems using Legendre polynomials, while Pooseh et al. [23] derived necessary optimality conditions for problems combining integer-order and fractional derivatives. Rabiei et al. [24] employed Boubaker polynomials for function discretization, and Heydari et al. [15] applied Legendre wavelets to solve a class of FOC problems. Alizadeh and Effati [7] proposed a variational iteration method, and Noori Skandari et al. [14,20] introduced fractional Chebyshev pseudospectral methods for FOC problems.

* Corresponding author e-mail: math.noori@yahoo.com

Fractional derivatives can be extended beyond constant orders to time-dependent variable orders, leading to variable-order fractional (VOF) calculus [22,27]. This generalization introduces computational challenges, as many relationships valid for constant fractional operators do not hold for variable-order cases, creating additional constraints and complexities.

Variable-order fractional optimal control (VOFOC) problems, defined using various VOF derivative definitions such as Riemann-Liouville and Caputo derivatives, present greater complexity compared to their fixed-order and classical counterparts. The behavior of variables, particularly control variables, requires careful analysis in these problems. Since analytical solutions are often infeasible due to high computational complexity, developing accurate numerical methods becomes essential.

Current numerical approaches for VOFOC problems remain limited. Zahra and Hikal [30] employed non-standard finite difference methods with reflection operator properties. Heydari [16] utilized Chebyshev cardinal functions and VOFD operational matrices to transform problems into algebraic systems. Heydari and Avazzadeh [17] developed a Legendre wavelet method with variable-order fractional integral operational matrices, while Bahaa et al. [9] derived Euler-Lagrange equations for VOFOC problems. Other approaches include Genocchi polynomials [29], Bernoulli polynomials for affine VOFOC problems [19], and fractional-order Bessel wavelet functions [10]. Moreover, Sweilam et al. [26] applied Pontryagin's maximum principle to a hybrid variable-order fractional coronavirus model. Additionally, [25] introduced Müntz-Legendre wavelets with an operational matrix based on regularized beta functions, transforming VOFOC problems into parameter optimization problems for enhanced accuracy and efficiency.

Despite these developments, there remains a need for convergent methods with simpler structures and reduced complexity. Given the global nature of fractional derivatives, spectral methods are particularly suitable for numerically solving continuous-time problems involving VOF differential equations. These methods offer the advantage of reducing problems to algebraic systems or nonlinear programming problems (NLPs) while maintaining high approximation accuracy.

Spectral and pseudospectral methods have recently gained traction for solving various continuous-time problems [12,21]. This article presents a shifted Legendre spectral-collocation (SLSC) method for numerically solving VOFOC problems, an approach not previously applied to this class of problems. We develop a new operational matrix for VOFD of shifted Legendre polynomials to transform problem constraints into algebraic equations, discretize the objective functional using quadrature formulas, and formulate a nonlinear programming problem to approximate optimal solutions. Under mild conditions, we establish the convergence of approximate solutions to exact solutions. Numerical results demonstrate the method's effectiveness for solving VOFOC problems.

The paper is organized as follows: Section 2 presents the necessary preliminaries; Section 3 derives the VOFD operational matrix for SL polynomials; Section 4 describes the SLSC method for discretizing VOFOC problems; Section 5 analyzes convergence; Section 6 provides numerical examples; and Section 7 presents conclusions and suggestions for future work.

2 Preliminaries

This section presents the fundamental definitions and mathematical preliminaries for fixed-order fractional derivatives, variable-order fractional derivatives (VOFDs) [8], and shifted Legendre (SL) polynomials [28].

2.1 Fixed-Order and Variable-Order Fractional Derivatives

Definition 1. *Let $X(\cdot)$ be defined on the finite interval $[0,T]$. The left and right Riemann-Liouville (RL) fractional integrals of fixed-order $\rho > 0$ are defined, respectively, as:*

$$ {}_0\mathbb{I}_t^{\rho} X(t) = \frac{1}{\Gamma(\rho)} \int_0^t (t-\tau)^{\rho-1} X(\tau) d\tau, \quad 0 < t, \tag{1}$$

$$ {}_t\mathbb{I}_T^{\rho} X(t) = \frac{1}{\Gamma(\rho)} \int_t^T (\tau-t)^{\rho-1} X(\tau) d\tau, \quad t < T. \tag{2}$$

Definition 2. *For a function $X(\cdot)$ on $[0,T]$, the left and right Caputo fractional derivatives of fixed-order $0 < \rho < 1$ are defined, respectively, as:*

$$ {}_0^C D_t^{\rho} X(t) = \frac{1}{\Gamma(1-\rho)} \int_0^t (t-\tau)^{-\rho} X'(\tau) d\tau, \quad 0 < t, \tag{3}$$

$$ {}_t^C D_T^{\rho} X(t) = \frac{-1}{\Gamma(1-\rho)} \int_t^T (\tau-t)^{-\rho} X'(\tau) d\tau, \quad t < T. \tag{4}$$

Definition 3. *Let $X : [0,T] \to \mathbb{R}$ be a continuously differentiable function and $\rho : [0,T] \to (0,1]$ be a continuous function. The left and right variable-order fractional (VOF) Caputo derivatives of $X(t)$ of order $\rho(t)$ are defined, respectively, by:*

$$ {}_0^C D_t^{\rho(t)} X(t) = \frac{1}{\Gamma(1-\rho(t))} \int_0^t (t-\tau)^{-\rho(t)} X'(\tau) d\tau, \tag{5}$$

$$ {}_t^C D_T^{\rho(t)} X(t) = \frac{-1}{\Gamma(1-\rho(t))} \int_t^T (\tau - t)^{-\rho(t)} X'(\tau) d\tau. \tag{6}$$

Lemma 1. *Let $X(t) = t^\gamma$ for $t \in [0,T]$ and $\gamma > 0$. Then*

$$ {}_0^C D_t^{\rho(t)} t^\gamma = \begin{cases} \dfrac{\Gamma(\gamma+1)}{\Gamma(\gamma-\rho(t)+1)} t^{\gamma-\rho(t)}, & \gamma \geq 1, \\ 0, & \gamma < 1. \end{cases} \tag{7}$$

This paper focuses exclusively on the left Caputo VOFD.

2.2 The Shifted Legendre Polynomials

The Legendre orthogonal polynomials on $[-1,1]$ are determined by the recurrence relation:

$$\begin{cases} L_{i+1}(\tau) = \dfrac{2i+1}{i+1} \tau L_i(\tau) - \dfrac{i}{i+1} L_{i-1}(\tau), & i \geq 1, \\ L_0(\tau) = 1, \quad L_1(\tau) = \tau, & \tau \in [-1,1]. \end{cases} \tag{8}$$

Applying the variable transformation $\tau = \frac{2}{T}t - 1$, the shifted Legendre (SL) polynomials on $[0,T]$ are generated by the recurrence relation:

$$\begin{cases} SL_{i+1}(t) = \dfrac{2i+1}{i+1} \left(\dfrac{2t}{T} - 1 \right) SL_i(t) - \dfrac{i}{i+1} SL_{i-1}(t), & i \geq 1, \\ SL_0(t) = 1, \quad SL_1(t) = \dfrac{2t}{T} - 1. \end{cases} \tag{9}$$

These polynomials satisfy the orthogonality condition:

$$\int_0^T SL_i(t) SL_j(t) dt = \begin{cases} \dfrac{T}{2i+1}, & i = j, \\ 0, & i \neq j. \end{cases} \tag{10}$$

The shifted Legendre polynomial of degree i has the analytic form:

$$SL_i(t) = \sum_{r=0}^{i} q_{i,r} t^r, \tag{11}$$

where the coefficients are given by:

$$q_{i,r} = (-1)^{i+r} \frac{(i+r)!}{(i-r)!(r!)^2 T^r}, \tag{12}$$

with the property:

$$SL_i(0) = (-1)^i, \quad SL_i(T) = 1.$$

3 Derivation of the Operational Matrix

Operational matrices serve as a cornerstone technique for the numerical solution of differential, integral, and integro-differential equations, transforming these problems into more manageable systems of algebraic equations. This section details the derivation of the operational matrix for the left Caputo VOFD of SL polynomials.

Any square-integrable function $\psi(\cdot) \in L_2[0,T]$ can be approximated by a finite series of $N+1$ SL polynomials:

$$\psi(t) \approx \psi_N(t) = \sum_{i=0}^{N} \eta_i SL_i(t),$$

which can be expressed compactly in vector form as:

$$\psi_N(t) = \boldsymbol{\eta}^T \bar{\boldsymbol{L}}_N(t),$$

where $\boldsymbol{\eta}^T = [\eta_0, \eta_1, \ldots, \eta_N]$ is the coefficient vector and $\bar{\boldsymbol{L}}_N(t) = [SL_0(t), SL_1(t), \ldots, SL_N(t)]^T$ is the vector of basis functions. To facilitate the derivation, we define the vector of monomial basis functions:

$$\boldsymbol{\Phi}_N(t) = [1, t, t^2, \ldots, t^N]^T, \quad 0 \le t \le T. \tag{13}$$

The vector of shifted Legendre polynomials can be represented as a linear transformation of this monomial basis:

$$\bar{\boldsymbol{L}}_N(t) = \boldsymbol{Q}\boldsymbol{\Phi}_N(t), \tag{14}$$

where $\boldsymbol{Q}$ is an $(N+1)\times(N+1)$ lower triangular transformation matrix:

$$\boldsymbol{Q} = \begin{bmatrix} q_{0,0} & 0 & 0 & \cdots & 0 \\ q_{1,0} & q_{1,1} & 0 & \cdots & 0 \\ \vdots & \vdots & \vdots & \ddots & \vdots \\ q_{N,0} & q_{N,1} & q_{N,2} & \cdots & q_{N,N} \end{bmatrix}. \tag{15}$$

Let $\rho(t) : [0,T] \to (0,1]$ define the variable fractional order. The next step is to find the left Caputo VOFD of the monomial vector $\boldsymbol{\Phi}_N(t)$. Applying Lemma 1 yields:

$${}_0^C D_t^{\rho(t)} \boldsymbol{\Phi}_N(t) = \left[0, \frac{\Gamma(2)}{\Gamma(2-\rho(t))} t^{1-\rho(t)}, \frac{\Gamma(3)}{\Gamma(3-\rho(t))} t^{2-\rho(t)}, \cdots, \frac{\Gamma(N+1)}{\Gamma(N+1-\rho(t))} t^{N-\rho(t)}\right]^T. \tag{16}$$

This result can be written as a matrix multiplication:

$${}_0^C D_t^{\rho(t)} \boldsymbol{\Phi}_N(t) = \boldsymbol{Y}^{\{\rho(t)\}} \boldsymbol{\Phi}_N(t), \tag{17}$$

where $\boldsymbol{Y}^{\{\rho(t)\}}$ is an $(N+1)\times(N+1)$ diagonal matrix given by:

$$\boldsymbol{Y}^{\{\rho(t)\}} = \operatorname{diag}\left(0, \frac{\Gamma(2)}{\Gamma(2-\rho(t))} t^{-\rho}, \frac{\Gamma(3)}{\Gamma(3-\rho(t))} t^{1-\rho}, \cdots, \frac{\Gamma(N+1)}{\Gamma(N+1-\rho(t))} t^{N-1-\rho}\right). \tag{18}$$

We now derive the VOFD for the shifted Legendre vector $\bar{\boldsymbol{L}}_N(t)$. Using equations (14) and (16), and noting that the matrix $\boldsymbol{Q}$ is constant, we obtain:

$$\mathbb{D}^{\rho(t)} \bar{\boldsymbol{L}}_N(t) = \mathbb{D}^{\rho(t)} (\boldsymbol{Q}\boldsymbol{\Phi}_N(t)) = \boldsymbol{Q}\left(\mathbb{D}^{\rho(t)} \boldsymbol{\Phi}_N(t)\right) = \boldsymbol{Q}\boldsymbol{Y}^{\{\rho(t)\}} \boldsymbol{\Phi}_N(t). \tag{19}$$

Since $\boldsymbol{Q}$ is invertible, we can substitute $\boldsymbol{\Phi}_N(t) = \boldsymbol{Q}^{-1} \bar{\boldsymbol{L}}_N(t)$ from (14) into (19):

$$\mathbb{D}^{\rho(t)} \bar{\boldsymbol{L}}_N(t) = \boldsymbol{Q}\boldsymbol{Y}^{\{\rho(t)\}} \left(\boldsymbol{Q}^{-1} \bar{\boldsymbol{L}}_N(t)\right) = \left(\boldsymbol{Q}\boldsymbol{Y}^{\{\rho(t)\}} \boldsymbol{Q}^{-1}\right) \bar{\boldsymbol{L}}_N(t).$$

This establishes the final form:

$$\mathbb{D}^{\rho(t)} \bar{\boldsymbol{L}}_N(t) = \boldsymbol{D}^{\{\rho(t)\}} \bar{\boldsymbol{L}}_N(t),$$

where the operational matrix $\boldsymbol{D}^{\{\rho(t)\}}$ for the variable-order fractional derivative is defined as:

$$\boldsymbol{D}^{\{\rho(t)\}} = \boldsymbol{Q}\boldsymbol{Y}^{\{\rho(t)\}} \boldsymbol{Q}^{-1}. \tag{20}$$

This operational matrix $\boldsymbol{D}^{\{\rho(t)\}}$ will be employed in the subsequent section to solve the given class of problems.

4 Discretization of the VOFOC Problem

In this section, we implement our approach on the following VOFOC problem:

$$\text{Minimize} \quad H(X(\cdot),U(\cdot)) = \int_0^T f(t,X(t),U(t))dt \tag{21}$$

$$\text{subject to} \quad \begin{cases} {}_0^C D_t^{\rho(t)} X(t) = h(t,X(t),U(t)), \quad 0 < t \le T, \\ X(0) = X_0, \end{cases} \tag{22}$$

where $X_0 \in \mathbb{R}$ is given, $f : \mathbb{R}\times\mathbb{R}^n\times\mathbb{R}^m \to \mathbb{R}$ and $h : \mathbb{R}\times\mathbb{R}^n\times\mathbb{R}^m \to \mathbb{R}$ are continuous functions, $X(t)$ and $U(t)$ are the state and control variables, respectively, $\rho : [0,T] \to (0,1]$ is a continuous function, and ${}_0^C D_t^{\rho(\cdot)}$ is the left Caputo VOFD operator. In the SLSC method, we approximate the variables of problem (21) and (22) in terms of the SL functions as follows:

$$X(t) \simeq X_N(t) = \boldsymbol{\eta}^T \bar{\boldsymbol{L}}_N(t), \quad U(t) \simeq U_N(t) = \boldsymbol{\gamma}^T \bar{\boldsymbol{L}}_N(t), \tag{23}$$

where $\boldsymbol{\eta}^T = [\eta_0, \eta_1, \cdots, \eta_N]$ and $\boldsymbol{\gamma}^T = [\gamma_0, \gamma_1, \cdots, \gamma_N]$ are unknown vectors to be computed. By (20) and (23), we obtain:

$${}_0^C D_t^{\rho(t)} X(t) \simeq {}_0^C D_t^{\rho(t)} \left(\boldsymbol{\eta}^T \bar{\boldsymbol{L}}_N(t)\right) = \boldsymbol{\eta}^T \left({}_0^C D_t^{\rho(t)} \bar{\boldsymbol{L}}_N(t)\right) = \boldsymbol{\eta}^T \boldsymbol{D}^{\{\rho(t)\}} \bar{\boldsymbol{L}}_N(t). \tag{24}$$

We will use the following theorem to approximate the objective functional (21).

Theorem 1. *Consider a polynomial $p(\cdot)$ of degree at most $(2N-1)$ on the interval $[0,T]$. We have the following quadrature formula:*

$$\int_0^T p(t)dt = \sum_{k=0}^{N} w_k p(t_k), \tag{25}$$

where $\{t_k\}_{k=0}^N$ are the roots of the polynomial $q(t) = t(T-t)SL_N'(t)$, and $w_k = \dfrac{T}{N(N+1)(SL_N(t_k))^2}$.

Proof. The result follows by applying the transformation $x = \frac{2t}{T} - 1$ in Theorem 3.29 of [28].

As a consequence of Theorem 1, for any continuous function $q(\cdot)$ on $[0,T]$, we obtain (see Lemma 2 in [13]):

$$\int_0^T q(t)dt = \lim_{N\to\infty} \sum_{k=0}^{N} w_k q(t_k). \tag{26}$$

Here $\{(t_k, w_k)\}_{k=0}^N$ is called the set of shifted Legendre-Gauss-Lobatto (SLGL) nodes and weights. Using relations (23) and (24), and Theorem 1, we can discretize the VOFOC problem (21)-(22) as follows:

$$\text{Minimize} \quad H_N(\boldsymbol{\eta},\boldsymbol{\gamma}) = \sum_{k=0}^{N} w_k f\left(t_k, \boldsymbol{\eta}^T \bar{\boldsymbol{L}}_N(t_k), \boldsymbol{\gamma}^T \bar{\boldsymbol{L}}_N(t_k)\right) \tag{27}$$

$$\text{subject to} \quad \begin{cases} \boldsymbol{\eta}^T \boldsymbol{D}^{\{\rho(t_k)\}} \bar{\boldsymbol{L}}_N(t_k) - h\left(t_k, \boldsymbol{\eta}^T \bar{\boldsymbol{L}}_N(t_k), \boldsymbol{\gamma}^T \bar{\boldsymbol{L}}_N(t_k)\right) = 0, \quad k = 1,2,\ldots,N, \\ \boldsymbol{\eta}^T \bar{\boldsymbol{L}}_N(t_0) - X_0 = 0, \end{cases} \tag{28}$$

where $\boldsymbol{\eta}^T = [\eta_0, \eta_1, \cdots, \eta_N]$ and $\boldsymbol{\gamma}^T = [\gamma_0, \gamma_1, \cdots, \gamma_N]$ are the unknown variables of the problem. By solving the NLP problem (27)-(28), we obtain an approximate solution for the main VOFOC problem (21)-(22).

5 Convergence Analysis

In this section, we analyze the convergence of the proposed method. We first rewrite problem (21)-(22) in the following equivalent form:

$$\text{Minimize} \quad H_N(\boldsymbol{\eta},\boldsymbol{\gamma}) = \sum_{k=0}^{N} w_k f\left(t_k, X_N(t_k), U_N(t_k)\right) \tag{29}$$

$$\text{subject to} \quad \begin{cases} {}_0^C D_t^{\rho(t_k)} X_N(t_k) - h(t_k, X_N(t_k), U_N(t_k)) = 0, \quad k = 1,\dots,N, \\ X_N(0) = X_0, \end{cases} \tag{30}$$

where $X_N(t_k) = \boldsymbol{\eta}^T \bar{\boldsymbol{L}}_N(t_k)$ and $U_N(t_k) = \boldsymbol{\gamma}^T \bar{\boldsymbol{L}}_N(t_k)$ for $k = 0,1,\dots,N$. We assume that problem (29)-(30) (or equivalently (27)-(28)) is feasible.

Lemma 2(See [28]). *For any function $\psi \in L_2([0,T])$, we have*

$$\psi(t) = \sum_{i=0}^{\infty} \lambda_i SL_i(t), \quad 0 \le t \le T,$$

where $SL_i(\cdot)$ is the SL polynomial defined by (9) and

$$\lambda_i = \frac{2i+1}{T} \int_0^T \psi(t) SL_i(t) dt. \tag{31}$$

Theorem 2. *Assume that $\{(\tilde{\boldsymbol{\eta}}_i, \tilde{\boldsymbol{\gamma}}_i)\}_{i=0}^N$ is the optimal solution of (27)-(28) and define*

$$\tilde{X}_N(t) = \sum_{i=0}^{N} \tilde{\eta}_i SL_i(t), \quad \tilde{U}_N(t) = \sum_{i=0}^{N} \tilde{\gamma}_i SL_i(t) \quad \text{on } [0,T].$$

Also, assume that $\{(\tilde{X}_N(\cdot), \tilde{U}_N(\cdot))\}_{N=N_0}^{\infty}$ uniformly converges to $(\tilde{X}(\cdot), \tilde{U}(\cdot))$ such that $\tilde{X}(\cdot)$ and $\tilde{U}(\cdot)$ are in $L_2([0,T])$ and ${}_0^C D_t^{\rho(t)} \tilde{X}(\cdot)$ is in $C((0,T])$. Then $(\tilde{X}(\cdot), \tilde{U}(\cdot))$ is an optimal solution for the main VOFOC problem (21)-(22).

Proof. We first show that $(\tilde{X}(\cdot), \tilde{U}(\cdot))$ is a feasible solution for the VOFOC problem (21)-(22). Let $t \in (0,T]$ be given. Since the SL points $\{t_k\}_{k=0}^N$ become dense on $[0,T]$ as $N \to \infty$, there exists a subsequence $\{t_{k_i}\}_{i=0}^{\infty}$ such that $\lim_{i\to\infty} k_i = \infty$ and $\lim_{i\to\infty} t_{k_i} = t$. By the continuity of functions $h(\cdot,\cdot,\cdot)$ and ${}_0^C D_t^{\rho(t)} \tilde{X}(\cdot)$, and constraint (30), we obtain:

$${}_0^C D_t^{\rho(t)} \tilde{X}(t) - h(t, \tilde{X}(t), \tilde{U}(t)) = \lim_{N\to\infty} \lim_{i\to\infty} \left({}_0^C D_t^{\rho(t_{k_i})} \tilde{X}_N(t_{k_i}) - h(t_{k_i}, \tilde{X}_N(t_{k_i}), \tilde{U}_N(t_{k_i})\right) = 0.$$

Also, for the initial condition:

$$\tilde{X}(0) - X_0 = \lim_{N\to\infty} (\tilde{X}_N(0) - X_0) = 0.$$

Now, we show that $(\tilde{X}(\cdot), \tilde{U}(\cdot))$ is an optimal solution. By the objective function (29):

$$H_N(\tilde{\boldsymbol{\eta}}, \tilde{\boldsymbol{\gamma}}) = \sum_{k=0}^{N} w_k f\left(t_k, \tilde{\boldsymbol{\eta}}^T \bar{\boldsymbol{L}}_N(t_k), \tilde{\boldsymbol{\gamma}}^T \bar{\boldsymbol{L}}_N(t_k)\right). \tag{32}$$

By the objective functional (21) and replacing the continuous function $q(\cdot)$ in relation (26) with $f(\cdot, \tilde{X}(\cdot), \tilde{U}(\cdot))$, we obtain:

$$H(\tilde{X}(\cdot), \tilde{U}(\cdot)) = \int_0^T f(t, \tilde{X}(t), \tilde{U}(t)) dt = \lim_{N\to\infty} \sum_{k=0}^{N} w_k f\left(t_k, \tilde{X}(t_k), \tilde{U}(t_k)\right). \tag{33}$$

Moreover, since $\sum_{k=0}^{N} w_k = T$ and $(\tilde{X}_N(\cdot), \tilde{U}_N(\cdot))$ uniformly converges to $(\tilde{X}(\cdot), \tilde{U}(\cdot))$, we have:

$$\begin{aligned}
&\lim_{N\to\infty}\left\|\sum_{k=0}^{N} w_k\left[f\left(t_k,\tilde{X}(t_k),\tilde{U}(t_k)\right) - f\left(t_k,\tilde{\boldsymbol{\eta}}^T\bar{\boldsymbol{L}}_N(t_k),\tilde{\boldsymbol{\gamma}}^T\bar{\boldsymbol{L}}_N(t_k)\right)\right]\right\|_\infty \\
&\leq L\lim_{N\to\infty}\sum_{k=0}^{N} w_k\left(\|\tilde{X}(t_k)-\tilde{\boldsymbol{\eta}}^T\bar{\boldsymbol{L}}_N(t_k)\|_\infty + \|\tilde{U}(t_k)-\tilde{\boldsymbol{\gamma}}^T\bar{\boldsymbol{L}}_N(t_k)\|_\infty\right) \\
&= L\lim_{N\to\infty}\sum_{k=0}^{N} w_k\left(\|\tilde{X}(t_k)-\tilde{X}_N(t_k)\|_\infty + \|\tilde{U}(t_k)-\tilde{U}_N(t_k)\|_\infty\right) \\
&\leq LT\lim_{N\to\infty}\left(\|\tilde{X}(\cdot)-\tilde{X}_N(\cdot)\|_\infty + \|\tilde{U}(\cdot)-\tilde{U}_N(\cdot)\|_\infty\right) = 0,
\end{aligned}$$

where $L > 0$ is the Lipschitz constant of the continuously differentiable function $f(\cdot,\cdot,\cdot)$. Thus, by (32) and (33), and the above result, we obtain:

$$\begin{aligned}
H(\tilde{X}(\cdot),\tilde{U}(\cdot)) &= \int_0^T f(t,\tilde{X}(t),\tilde{U}(t))dt \\
&= \lim_{N\to\infty}\Bigg(\sum_{k=0}^{N} w_k f\left(t_k,\tilde{\boldsymbol{\eta}}^T\bar{\boldsymbol{L}}_N(t_k),\tilde{\boldsymbol{\gamma}}^T\bar{\boldsymbol{L}}_N(t_k)\right) \\
&\quad + \sum_{k=0}^{N} w_k\left[f\left(t_k,\tilde{X}(t_k),\tilde{U}(t_k)\right) - f\left(t_k,\tilde{\boldsymbol{\eta}}^T\bar{\boldsymbol{L}}_N(t_k),\tilde{\boldsymbol{\gamma}}^T\bar{\boldsymbol{L}}_N(t_k)\right)\right]\Bigg) \\
&= \lim_{N\to\infty}\sum_{k=0}^{N} w_k f\left(t_k,\tilde{\boldsymbol{\eta}}^T\bar{\boldsymbol{L}}_N(t_k),\tilde{\boldsymbol{\gamma}}^T\bar{\boldsymbol{L}}_N(t_k)\right) = \lim_{N\to\infty} H_N(\tilde{\boldsymbol{\eta}},\tilde{\boldsymbol{\gamma}}).
\end{aligned}$$

Hence,

$$H(\tilde{X}(\cdot),\tilde{U}(\cdot)) = \lim_{N\to\infty} H_N(\tilde{\boldsymbol{\eta}},\tilde{\boldsymbol{\gamma}}). \tag{34}$$

By Lemma 2, for any optimal solution $(X^*(\cdot),U^*(\cdot))$ of problem (21)-(22), there exists a corresponding sequence $\{(\eta_i^*,\gamma_i^*)\}_{i=0}^{\infty}$. Since $(X^*(\cdot),U^*(\cdot))$ satisfies constraint (22), the sequence $\{(\eta_i^*,\gamma_i^*)\}_{i=0}^{N}$ with $N\to\infty$ satisfies constraint (30). Similar to the derivation of (34), we have:

$$H(X^*(\cdot),U^*(\cdot)) = \lim_{N\to\infty} H_N(\boldsymbol{\eta}^*,\boldsymbol{\gamma}^*), \tag{35}$$

where $\boldsymbol{\eta}^* = (\eta_0^*,\eta_1^*,\ldots,\eta_N^*)$ and $\boldsymbol{\gamma}^* = (\gamma_0^*,\gamma_1^*,\ldots,\gamma_N^*)$. By relations (34) and (35), and the optimality of pairs $(\tilde{\boldsymbol{\eta}},\tilde{\boldsymbol{\gamma}})$ and $(X^*(\cdot),U^*(\cdot))$, we obtain:

$$H(X^*(\cdot),U^*(\cdot)) \leq H(\tilde{X}(\cdot),\tilde{U}(\cdot)) = \lim_{N\to\infty} H_N(\tilde{\boldsymbol{\eta}},\tilde{\boldsymbol{\gamma}}) \leq \lim_{N\to\infty} H_N(\boldsymbol{\eta}^*,\boldsymbol{\gamma}^*) = H(X^*(\cdot),U^*(\cdot)),$$

which implies $H(X^*(\cdot),U^*(\cdot)) = H(\tilde{X}(\cdot),\tilde{U}(\cdot))$. Thus, $(\tilde{X}(\cdot),\tilde{U}(\cdot))$ is an optimal solution for the VOFOC problem (21)-(22).

6 Numerical Examples

This section presents numerical solutions for six VOFOC problems. We employ the fmincon solver in MATLAB to solve the corresponding NLP problems given by relations (27)-(28). The absolute errors of the approximate solutions are calculated using:

$$E_X(t) = |X(t)-X^*(t)|, \quad E_U(t) = |U(t)-U^*(t)|, \quad 0 \leq t \leq T,$$

where (X,U) and (X^*,U^*) denote the approximate and exact optimal solutions, respectively. The step-by-step procedure for implementing the proposed SLSC method is as follows:

Algorithm 1: SLSC Method for VOFOC Problems

Input: Problem data: T, X_0, functions f, h, and $\rho(t)$; Discretization parameter: N.

Output: Approximate optimal state $X_N(t)$, control $U_N(t)$, and cost functional H_N.

Step 1: Precompute basis and quadrature

1-1: Generate the $N+1$ shifted Legendre polynomials $\{SL_i(t)\}_{i=0}^N$ on $[0,T]$ using recurrence relation (9).

1-2: Compute the $(N+1)\times(N+1)$ transformation matrix Q and its inverse Q^{-1} using (12) and (15).

1-3: Compute the SLGL nodes $\{t_k\}_{k=0}^N$ and weights $\{w_k\}_{k=0}^N$ on $[0,T]$ as per Theorem 1.

Step 2: Construct the operational matrix

2-1: For each SLGL node t_k, compute the diagonal matrix: $Y^{\{\rho(t_k)\}}$ using (18).

2-2: For each t_k, compute the VOFD operational matrix: $D^{\{\rho(t_k)\}} = QY^{\{\rho(t_k)\}}Q^{-1}$.

Step 3: Formulate the NLP problem

3-1: Define decision variables: $\boldsymbol{\eta} = [\eta_0,\dots,\eta_N]^T$, $\boldsymbol{\gamma} = [\gamma_0,\dots,\gamma_N]^T$.

3-2: Formulate objective function $H_N(\boldsymbol{\eta},\boldsymbol{\gamma})$ from (27).

3-3: Formulate constraints from (28).

Step 4: Solve the NLP Problem

4-1: Use `fmincon` in MATLAB to solve: $\min_{\boldsymbol{\eta},\boldsymbol{\gamma}} H_N(\boldsymbol{\eta},\boldsymbol{\gamma})$ subject to the constraints.

4-2: Provide initial guess (e.g., zero vectors).

Step 5: Reconstruct the Solution

5-1 Extract optimal coefficients $\boldsymbol{\eta}^*$ and $\boldsymbol{\gamma}^*$.

5-2 Reconstruct solutions: $X_N(t) = (\boldsymbol{\eta}^*)^T\bar{L}_N(t)$, $U_N(t) = (\boldsymbol{\gamma}^*)^T\bar{L}_N(t)$.

5-3 Compute optimal cost: $H_N(\boldsymbol{\eta}^*,\boldsymbol{\gamma}^*)$.

*Example 1.*Consider the following VOFOC problem:

$$\text{Minimize} \quad H = \int_0^1 \left[(X(t)-t^2)^2 + (U(t)-e^{-t})^2\right] dt$$

$$\text{subject to} \quad \begin{cases} {}_0^C D_t^{\rho(t)} X(t) = U^2(t) - e^{-2t} + 2t, & 0 < t \le 1, \\ X(0) = 0. \end{cases}$$

The exact optimal solution for $\rho(t)=1$ is $(X^*,U^*) = (t^2, e^{-t})$, with the corresponding optimal value $H^*=0$. We apply the proposed method to solve this problem. The discretized NLP problem, derived from relations (27) and (28), is formulated as:

$$\text{Minimize} \quad H_N = \sum_{j=0}^N w_j \left[\left(\sum_{i=0}^N \eta_i SL_i(t_j) - t_j^2\right)^2 + \left(\sum_{i=0}^N \gamma_i SL_i(t_j) - e^{-t_j}\right)^2\right]$$

$$\text{subject to} \quad \begin{cases} \sum_{i=0}^N \eta_i D^{\rho}_{r,i+1} - \left(\sum_{i=0}^N \gamma_i SL_i(t_r)\right)^2 + e^{-2t_r} - 2t_r = 0, & r = 1,2,\dots,N, \\ \sum_{i=0}^N \eta_i SL_i(0) = 0, \end{cases}$$

where (η_i, γ_i) for $i = 0,1,\ldots,N$ are the unknown coefficients, and $D^{\rho}_{r,i+1}$ for $i = 0,1,\ldots,N$ are the components of the vector $\boldsymbol{D}^{\{\rho(t_r)\}}\bar{\boldsymbol{L}}(t_r)$ for $r = 1,2,\ldots,N$. We solve this NLP for $N = 5$ and various functions $\rho(\cdot)$. The approximate optimal solutions are illustrated in Figures 1, 2, and 3. The absolute error for the case $\rho(t) = 1$ with $N = 5,6$ is presented in Figure 4, demonstrating that the error decreases as the number of basis polynomials increases. The computed values of the objective functional H_N are listed in Tables 1, 2, and 3. The results show that as $\rho(\cdot)$ approaches 1, the approximate solutions converge to the exact solution corresponding to $\rho(t) = 1$.

*Example 2.*Consider the VOFOC problem:

$$\text{Minimize} \quad H = \int_0^1 \left[(X(t)-t)^2 + (U(t)-t-1)^2\right] dt$$

$$\text{subject to} \quad \begin{cases} {}_0^C D_t^{\rho(t)} X(t) = -X(t) + U(t), & 0 < t \le 1, \\ X(0) = 0. \end{cases}$$

The exact optimal solution for $\rho(t) = 1$ is $(X^*, U^*) = (t, t+1)$. We solve this problem for $N = 5$ and different functions $\rho(\cdot)$. The approximate optimal solutions are shown in Figures 5 and 6. The corresponding values of H_N are provided in Tables 5 and 6. Figure 7 displays the absolute error for $\rho(t) = 1$ with $N = 5,6$, showing a decrease in error with increasing N. These results indicate that accurate approximate solutions are achievable with a small number of collocation points. Furthermore, the approximate solutions for different $\rho(\cdot)$ converge to the exact solution as $\rho(\cdot)$ approaches 1.

*Example 3.*Consider the VOFOC problem:

$$\text{Minimize} \quad H = \int_0^1 \left[(X(t)-e^{-t})^2 + (U(t)-t^3)^2\right] dt$$

$$\text{subject to} \quad \begin{cases} {}_0^C D_t^{\rho(t)} X(t) = -X^2(t) + U^2(t) - t^6 - e^{-t} + e^{-2t}, & 0 < t \le 1, \\ X(0) = 0. \end{cases}$$

The exact optimal solution for $\rho(t) = 1$ is $(X^*, U^*) = (e^{-t}, t^3)$. We apply our method for different functions $\rho(\cdot)$. The approximate optimal solutions for $N = 6$ are shown in Figures 8 and 9. The absolute error for $\rho(t) = 1$ is illustrated in Figure 10, indicating that the approximate solution is a good approximation of the exact one. The obtained values of H_N for $N = 6$ are given in Tables 7 and 8. The results confirm that as $\rho(\cdot)$ tends to 1, the approximate solutions approach the exact optimal solution.

*Example 4.*Consider the VOFOC problem:

$$\text{Minimize} \quad H = \int_0^1 \left[(X(t)-\rho(t))^2 + (U(t)-\sin(\pi\rho(t)))^2\right] dt$$

$$\text{subject to} \quad \begin{cases} {}_0^C D_t^{\rho(t)} X(t) = \dfrac{\Gamma(\beta+1)}{\Gamma(\beta+1-\rho(t))} t^{\beta-\rho(t)} + U^2(t) + \cos^2(\pi\rho(t)) - 1, & 0 < t \le 1, \\ X(0) = 0, \end{cases}$$

where $\rho(t) = t^{\beta}$ with $\beta \ge 1$. The exact optimal solution is $(X^*, U^*) = (\rho(t), \sin(\pi\rho(t)))$, with $H^* = 0$. We apply our method with $N = 8$ and compare the results with the exact solution. The results for $\beta = 1,2,3,4$ are illustrated in Figures 11 and 12. The approximate values of H are shown in Table 9. This example demonstrates the effectiveness and applicability of our approach for solving VOFOC problems.

*Example 5.*Consider the problem of controlling train motion to minimize energy consumption, modeled as a VOFOC problem for greater realism:

$$\text{Minimize} \quad H = \frac{1}{2}\int_0^1 U^2(t) dt$$

$$\text{subject to} \quad \begin{cases} {}_0^C D_t^{\rho(t)} X_1(t) = X_2(t), & 0 < t \le 1, \\ {}_0^C D_t^{\rho(t)} X_2(t) = U(t), & 0 < t \le 1, \\ X_1(0) = 1, \quad X_2(0) = 1, \\ X_1(1) = 0, \quad X_2(1) = 0, \end{cases}$$

where $X_1(\cdot)$ and $X_2(\cdot)$ represent the position and velocity of the train, respectively, and $U(\cdot)$ is the control (energy) variable. The exact optimal solutions for $\rho(t)=1$ is $X_1^*(t)=3t^3-5t^2+t+1$, $X_2^*(t)=9t^2-10t+1$, and $U^*(t)=18t-10$. We apply our method for different functions $\rho(\cdot)$ with $N=5$. The approximate optimal state and control variables are shown in Figures 13–18. The corresponding values of H_N are listed in Tables 4–11. The results show that as $\rho(\cdot)$ approaches 1, the numerical solutions converge to the exact optimal solution, and good accuracy is achieved even for $N=5$.

*Example 6.*Consider the VOFOC problem:

$$\text{Minimize} \quad H=\int_0^1 \left[X^2(t)+U^2(t)\right]dt$$

$$\text{subject to} \quad \begin{cases} {}_0^C D_t^{\rho(t)}X(t)=-X(t)+U(t), & 0<t\leq 1, \\ X(0)=0. \end{cases}$$

The exact optimal solution for $\rho(t)=1$ is:

$$\begin{cases} X^*(t)=\cosh(\sqrt{2}t)+\beta\sinh(\sqrt{2}t), \\ U^*(t)=(1+\sqrt{2}\beta)\cosh(\sqrt{2}t)+(\sqrt{2}+\beta)\sinh(\sqrt{2}t), \end{cases}$$

where $\beta=-\dfrac{\cosh(\sqrt{2})+\sqrt{2}\sinh(\sqrt{2})}{\sqrt{2}\cosh(\sqrt{2})+\sinh(\sqrt{2})}$, and the optimal performance index is $H^*=0.192909298093$. We apply our method for different functions $\rho(\cdot)$. The approximate optimal solutions for $N=5$ are shown in Figures 19–21. The absolute error for $\rho(t)=1$ with $N=3,5,7$ is illustrated in Figure 22, showing that the approximate solution is a good approximation of the exact one. Tables 12 and 13 compare the absolute errors of our method with other methods from the literature for $\rho=1$, demonstrating the superior accuracy of our approach. Furthermore, Table 14 presents the approximate values of the objective functional H_N for $\rho=1$, showing that our method converges to H^* with high accuracy and outperforms the method in [14].

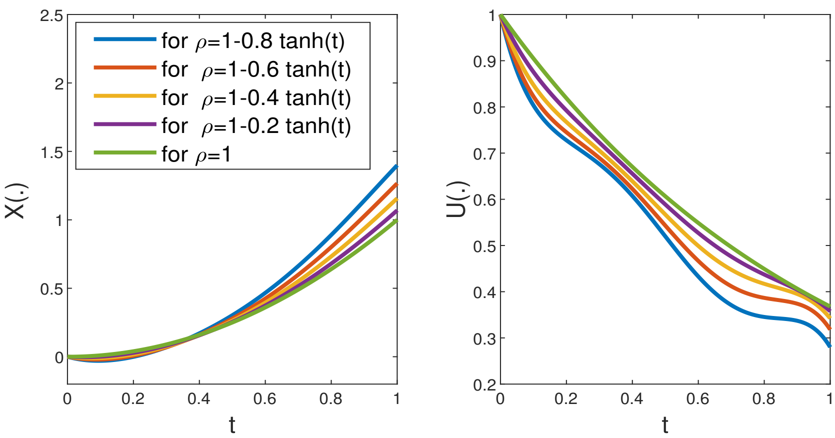

Fig. 1: Approximate optimal solution for Example 1 with $\rho(t)=1-\beta\tanh(t)$ for $\beta=0,0.2,0.4,0.6,0.8$.

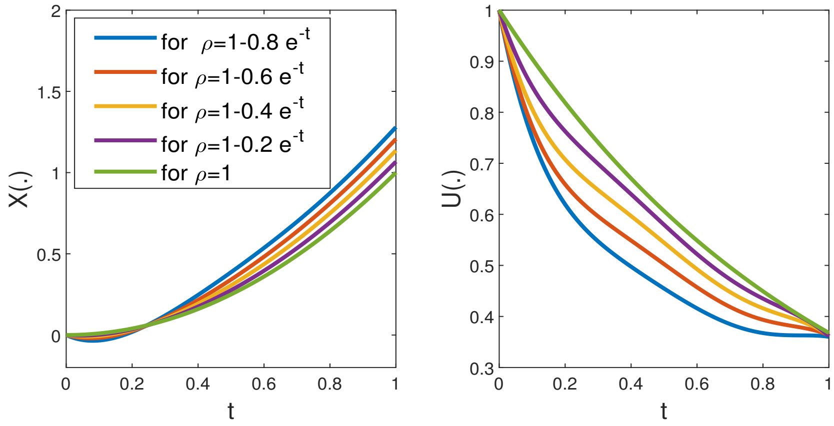

Fig. 2: Approximate optimal solution for Example 1 with $\rho(t) = 1 - \beta e^{-t}$ for $\beta = 0, 0.2, 0.4, 0.6, 0.8$.

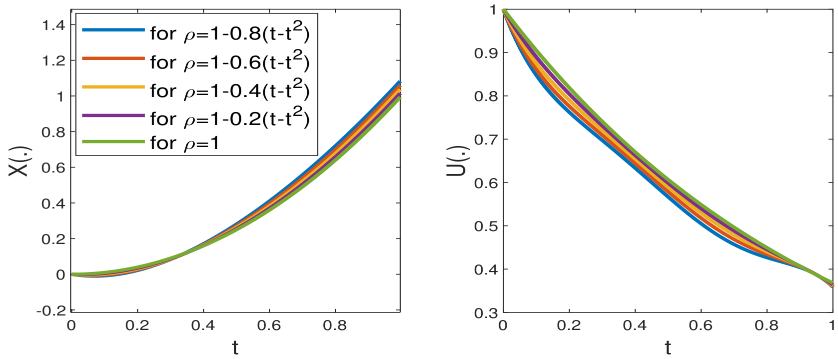

Fig. 3: Approximate optimal solution for Example 1 with $\rho(t) = 1 - \beta(t - t^2)$ for $\beta = 0, 0.2, 0.4, 0.6, 0.8$.

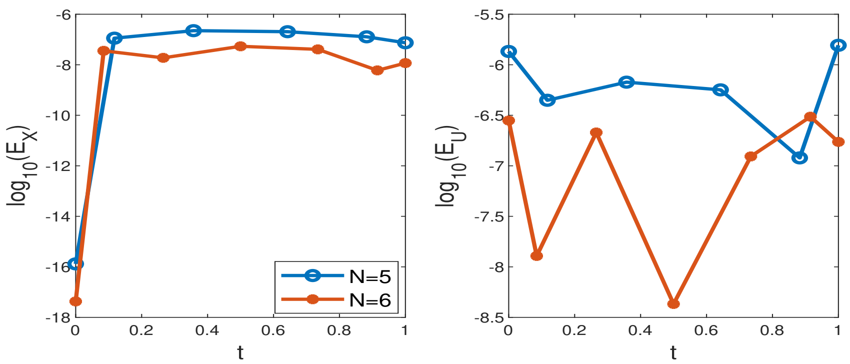

Fig. 4: Logarithm of absolute error for Example 1 with $\rho(t) = 1$.

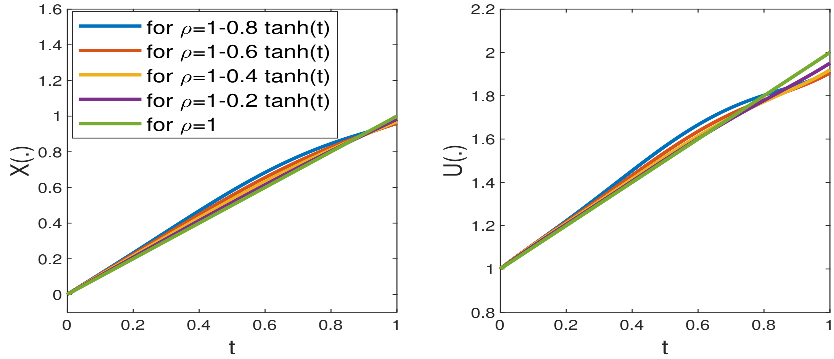

Fig. 5: Approximate optimal solution for Example 2 with $\rho(t) = 1 - \beta \tanh(t)$ for $\beta = 0, 0.2, 0.4, 0.6, 0.8$.

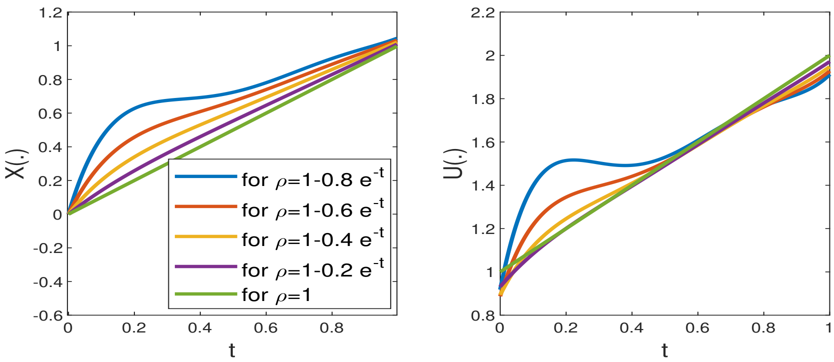

Fig. 6: Approximate optimal solution for Example 2 with $\rho(t) = 1 - \beta e^{-t}$ for $\beta = 0, 0.2, 0.4, 0.6, 0.8$.

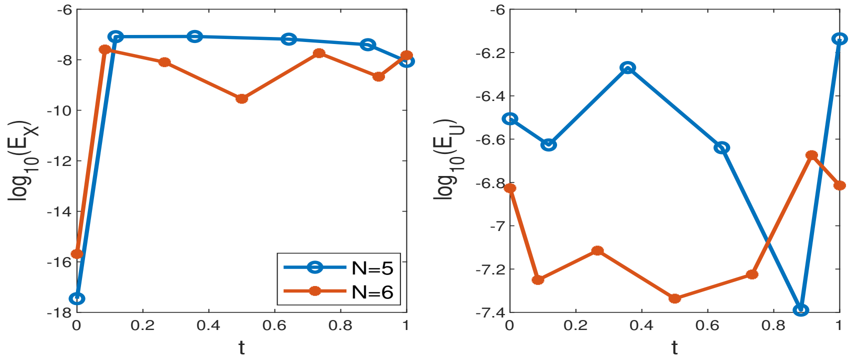

Fig. 7: Logarithm of absolute error for Example 2 with $\rho(t) = 1$.

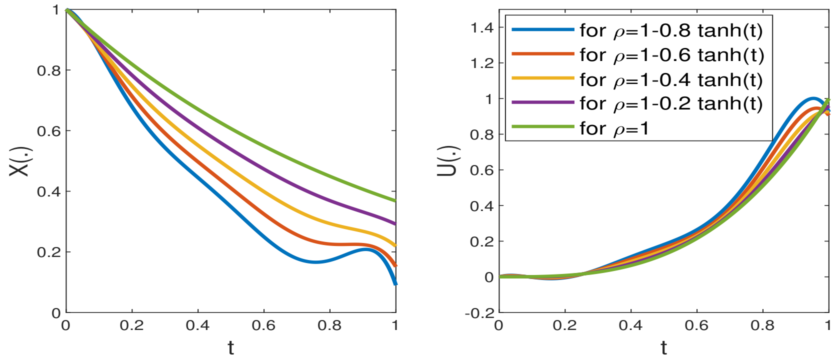

Fig. 8: Approximate optimal solution for Example 3 with $\rho(t) = 1 - \beta \tanh(t)$ for $\beta = 0, 0.2, 0.4, 0.6, 0.8$.

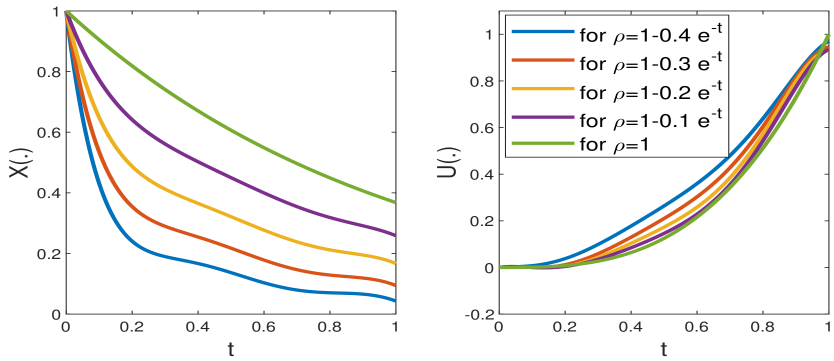

Fig. 9: Approximate optimal solution for Example 3 with $\rho(t) = 1 - \beta e^{-t}$ for $\beta = 0, 0.1, 0.2, 0.3, 0.4$.

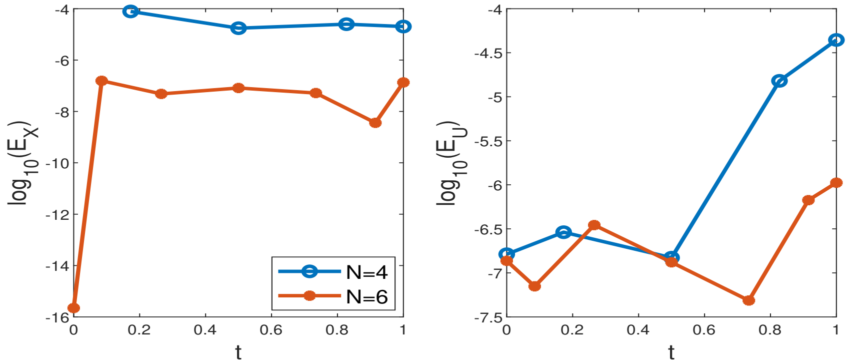

Fig. 10: Logarithm of absolute error for Example 3 with $\rho(t) = 1$.

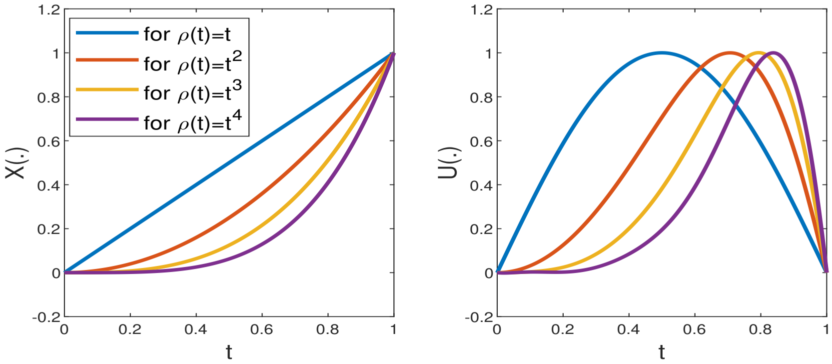

Fig. 11: Approximate optimal solution for Example 4.

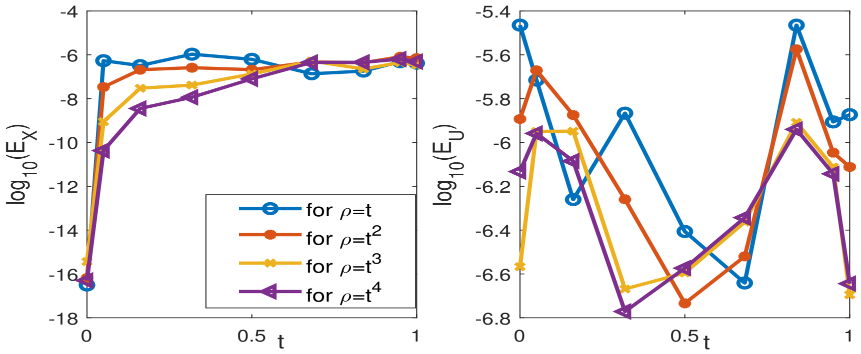

Fig. 12: Logarithm of absolute error for Example 4 with $N = 8$.

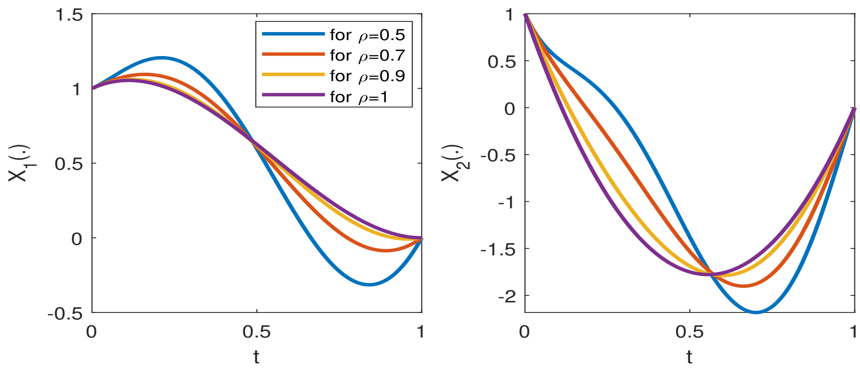

Fig. 13: Approximate optimal state variable for Example 5 with $\rho(t) = 0.5, 0.7, 0.9, 1$.

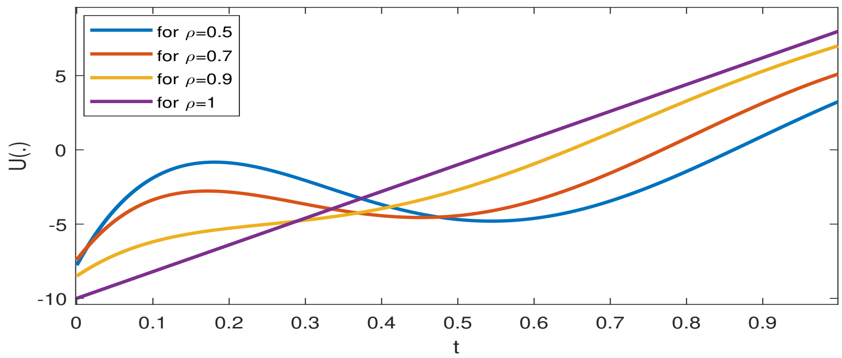

Fig. 14: Approximate optimal control variable for Example 5 with $\rho(t) = 0.5, 0.7, 0.9, 1$.

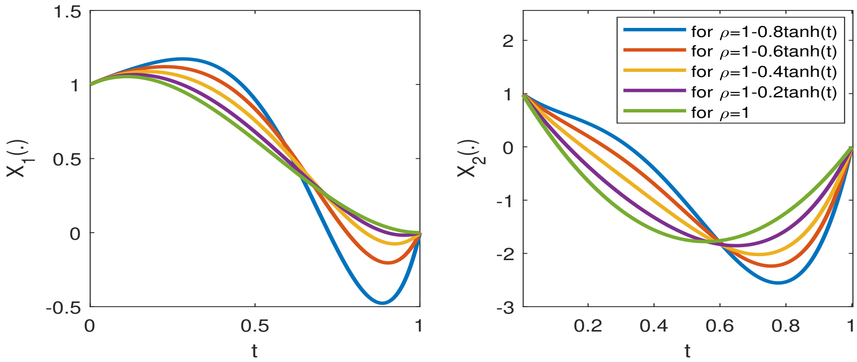

Fig. 15: Approximate optimal state variable for Example 5 with $\rho(t) = 1 - \beta \tanh(t)$ for $\beta = 0, 0.2, 0.4, 0.6, 0.8$.

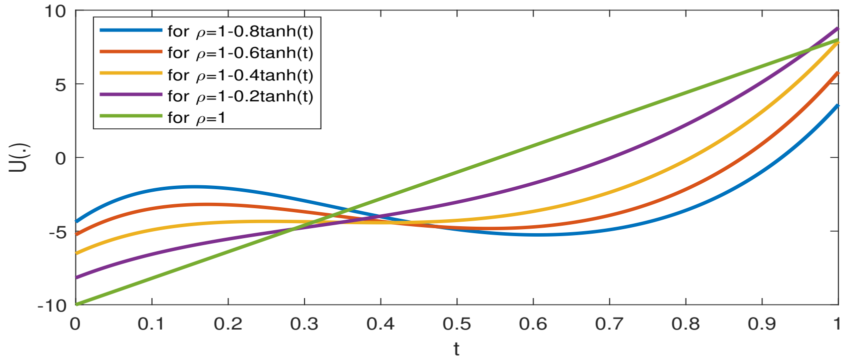

Fig. 16: Approximate optimal control variable for Example 5 with $\rho(t) = 1 - \beta \tanh(t)$ for $\beta = 0, 0.2, 0.4, 0.6, 0.8$.

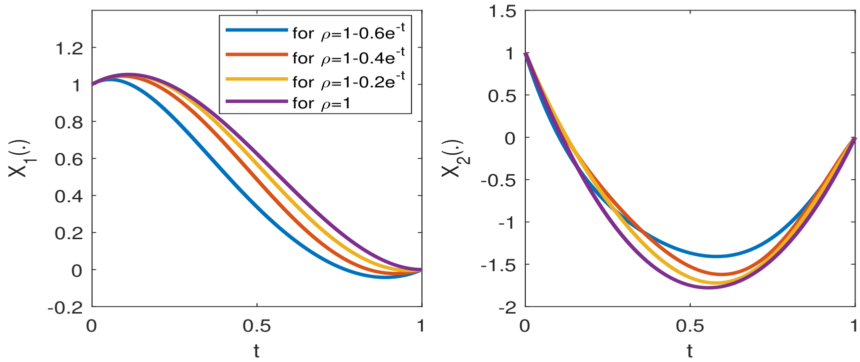

Fig. 17: Approximate optimal state variable for Example 5 with $\rho(t) = 1 - \beta e^{-t}$ for $\beta = 0, 0.2, 0.4, 0.6$.

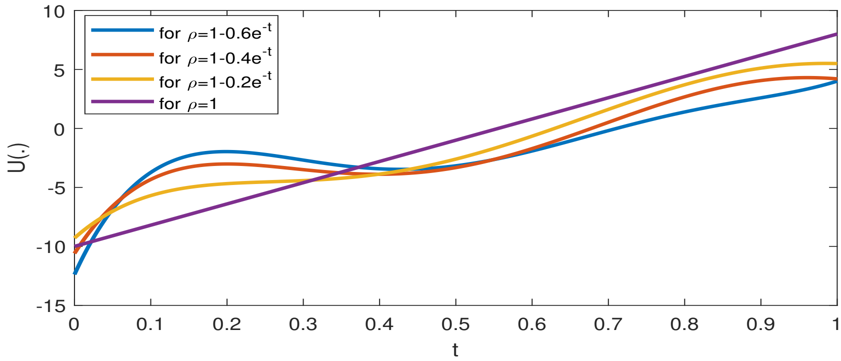

Fig. 18: Approximate optimal control variable for Example 5 with $\rho(t) = 1 - \beta e^{-t}$ for $\beta = 0, 0.2, 0.4, 0.6$.

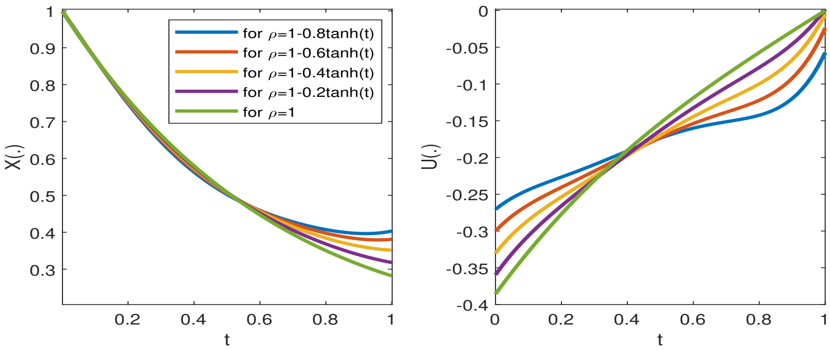

Fig. 19: Approximate optimal solution for Example 6 with $\rho(t) = 1 - \beta \tanh(t)$ for $\beta = 0, 0.2, 0.4, 0.6, 0.8$.

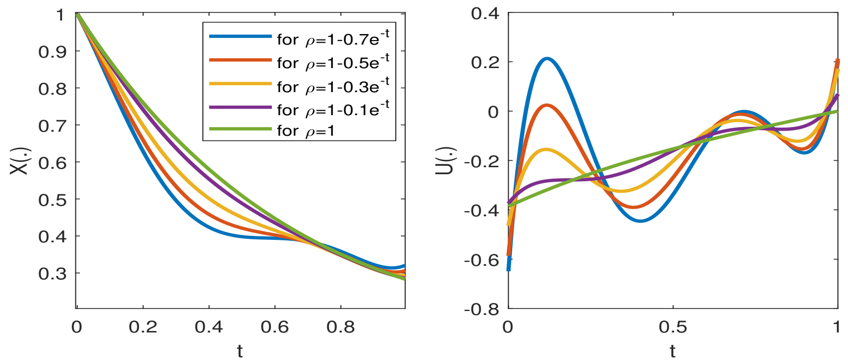

Fig. 20: Approximate optimal solution for Example 6 with $\rho(t) = 1 - \beta e^{-t}$ for $\beta = 0, 0.2, 0.4, 0.6, 0.8$.

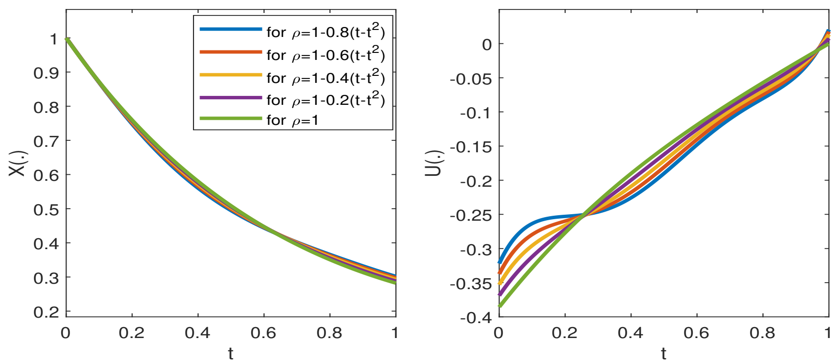

Fig. 21: Approximate optimal solution for Example 6 with $\rho(t) = 1 - \beta(t - t^2)$ for $\beta = 0, 0.2, 0.4, 0.6, 0.8$.

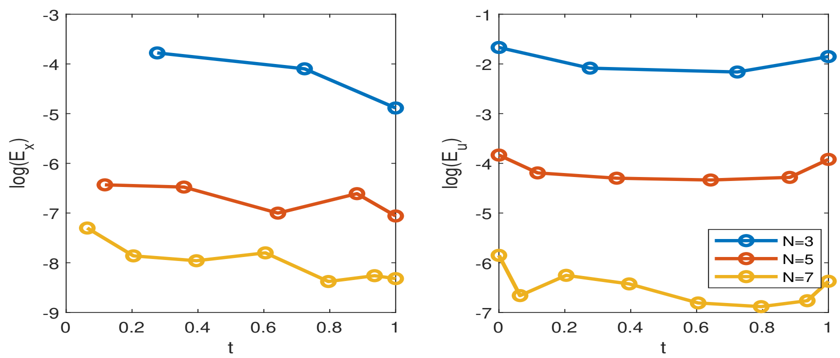

Fig. 22: Logarithm of absolute error for Example 6 with $\rho(t) = 1$.

$N=5$	$\beta=0.8$	$\beta=0.6$	$\beta=0.4$	$\beta=0.2$	$\beta=0$
H_N	3.812×10^{-2}	1.697×10^{-2}	5.985×10^{-2}	1.193×10^{-3}	4.273×10^{-13}

Table 1: Optimal values of the objective functional H for Example 1 with $\rho(t)=1-\beta\tanh(t)$.

$N=5$	$\beta=0.8$	$\beta=0.6$	$\beta=0.4$	$\beta=0.2$	$\beta=0$
H_N	4.571×10^{-2}	2.440×10^{-2}	1.034×10^{-2}	2.254×10^{-3}	4.273×10^{-13}

Table 2: Optimal values of the objective functional H for Example 1 with $\rho(t)=1-\beta e^{-t}$.

$N=5$	$\beta=0.8$	$\beta=0.6$	$\beta=0.4$	$\beta=0.2$	$\beta=0$
H_N	4.254×10^{-3}	2.256×10^{-3}	9.428×10^{-4}	2.209×10^{-4}	4.273×10^{-13}

Table 3: Optimal values of the objective functional H for Example 1 with $\rho(t)=1-\beta(t-t^2)$.

$\rho(t)$	$1-0.8\tanh(t)$	$1-0.6\tanh(t)$	$1-0.4\tanh(t)$	$1-0.2\tanh(t)$	$\rho(t)=1$
H_N	6.6973	7.1716	8.5857	10.9632	14

Table 4: Optimal values of the objective functional H for Example 5 with $N=5$.

$N=5$	$\beta=0.8$	$\beta=0.6$	$\beta=0.4$	$\beta=0.2$	$\beta=0$
H_N	2.894×10^{-3}	1.967×10^{-3}	1.011×10^{-3}	2.819×10^{-4}	1.313×10^{-13}

Table 5: Optimal values of the objective functional H for Example 2 with $\rho(t)=1-\beta\tanh(t)$.

$N=5$	$\beta=0.8$	$\beta=0.6$	$\beta=0.4$	$\beta=0.2$	$\beta=0$
H_N	2.361×10^{-3}	1.356×10^{-3}	5.661×10^{-4}	1.269×10^{-4}	1.313×10^{-13}

Table 6: Optimal values of the objective functional H for Example 2 with $\rho(t)=1-\beta e^{-t}$.

$N=6$	$\beta=0.8$	$\beta=0.6$	$\beta=0.4$	$\beta=0.2$	$\beta=0$
H_N	5.962×10^{-2}	3.514×10^{-2}	1.621×10^{-2}	4.179×10^{-3}	1.273×10^{-13}

Table 7: Optimal values of the objective functional H for Example 3 with $\rho(t)=1-\beta\tanh(t)$.

$N=6$	$\beta=0.4$	$\beta=0.3$	$\beta=0.2$	$\beta=0.1$	$\beta=0$
H_N	2.12×10^{-1}	1.408×10^{-1}	7.377×10^{-2}	2.177×10^{-2}	1.273×10^{-13}

Table 8: Optimal values of the objective functional H for Example 3 with $\rho(t)=1-\beta e^{-t}$.

$N=8$	$\rho(t)=t$	$\rho(t)=t^2$	$\rho(t)=t^3$	$\rho(t)=t^4$
H	2.97×10^{-12}	1.92×10^{-12}	6.65×10^{-13}	5.79×10^{-13}

Table 9: Optimal values of the objective functional H for Example 4.

β	$\beta=0.6$	$\beta=0.4$	$\beta=0.2$	$\beta=0$
H	5.8829	7.1020	9.4310	14

Table 10: Optimal values of the objective functional H for Example 5 with $\rho(t)=1-\beta e^{-t}$.

$\rho(t)$	$\rho(t)=0.5$	$\rho(t)=0.7$	$\rho(t)=0.9$	$\rho(t)=1$
H_N	5.1692	6.4129	10.3422	14

Table 11: Optimal values of the objective functional H for Example 5 with $N=5$.

Time	Method [7] $N=30$	Method [18] $m=5$	Method [15] $\hat{m}=40$	Method [14] $N=5$	Suggested Method $N=5$
0.1	4.08×10^{-5}	1.34×10^{-5}	3.31×10^{-5}	2.11×10^{-5}	7.37×10^{-7}
0.2	8.26×10^{-5}	2.12×10^{-5}	2.91×10^{-5}	9.71×10^{-6}	4.29×10^{-6}
0.3	1.26×10^{-4}	3.24×10^{-5}	4.51×10^{-6}	4.08×10^{-7}	3.04×10^{-6}
0.4	1.72×10^{-4}	4.73×10^{-5}	5.41×10^{-6}	5.76×10^{-7}	1.73×10^{-6}
0.5	2.21×10^{-4}	6.20×10^{-5}	1.41×10^{-4}	5.66×10^{-6}	4.23×10^{-6}
0.6	2.73×10^{-4}	7.49×10^{-5}	1.88×10^{-5}	9.25×10^{-6}	1.99×10^{-6}
0.7	3.28×10^{-4}	8.88×10^{-5}	2.49×10^{-5}	8.35×10^{-6}	2.36×10^{-6}
0.8	3.86×10^{-4}	1.07×10^{-4}	3.96×10^{-5}	4.34×10^{-6}	3.51×10^{-6}
0.9	4.46×10^{-4}	1.31×10^{-4}	3.95×10^{-5}	2.59×10^{-6}	6.57×10^{-7}

Table 12: Absolute error of approximate optimal state variable for Example 6 with $\rho(t)=1$.

Time	VI Method [7] $N=30$	Wavelet Method [15] $\hat{m}=40$	Chebyshev PS Method [14] $N=5$	Suggested Method $N=5$
0.1	2.80×10^{-4}	7.64×10^{-5}	6.74×10^{-6}	6.09×10^{-5}
0.2	2.95×10^{-4}	5.61×10^{-5}	3.17×10^{-6}	2.60×10^{-5}
0.3	2.94×10^{-4}	3.98×10^{-6}	5.92×10^{-7}	3.71×10^{-5}
0.4	2.79×10^{-6}	2.74×10^{-6}	7.10×10^{-7}	4.63×10^{-5}
0.5	2.51×10^{-4}	1.82×10^{-4}	2.01×10^{-6}	5.29×10^{-6}
0.6	2.13×10^{-4}	1.16×10^{-5}	2.71×10^{-6}	3.90×10^{-5}
0.7	1.67×10^{-4}	7.16×10^{-6}	2.11×10^{-6}	3.86×10^{-5}
0.8	1.15×10^{-4}	4.65×10^{-6}	8.59×10^{-7}	1.48×10^{-5}
0.9	5.87×10^{-5}	4.16×10^{-5}	8.93×10^{-8}	5.06×10^{-5}

Table 13: Absolute error of approximate optimal control variable for Example 6 with $\rho(t)=1$.

N	H by [14]	H by Suggested method	$\|H-H^*\|$ by [14]	$\|H-H^*\|$ by our method
2	0.208449074074	0.196581196581	1.55×10^{-2}	3.67×10^{-3}
3	0.194344526028	0.192956016968	1.43×10^{-2}	4.67×10^{-5}
4	0.192988105760	0.192909658108	7.88×10^{-5}	3.60×10^{-7}
5	0.192914235995	0.192909299828	4.93×10^{-6}	1.73×10^{-9}
6	0.192909514139	0.192909298102	2.16×10^{-7}	8.99×10^{-12}
7	0.192909308499	0.192909298093	1.04×10^{-8}	0

Table 14: Approximate optimal values of the objective functional H for Example 6.

7 Conclusion and Future Work

This paper has successfully developed and validated a direct numerical method for the approximate solution of VOFOC problems. The technique is built upon the powerful framework of SL polynomials, leveraging their excellent spectral accuracy and orthogonality properties. The cornerstone of our methodology is the newly derived operational matrix for the Caputo-type VOFD, which allows for an elegant and precise discretization of the fractional dynamical constraints. The numerical results from a diverse set of six examples unequivocally demonstrate the strength of our approach. Key findings include: i) The method produces highly accurate approximations of both state and control variables, often matching the exact solution for integer-order cases to machine precision, even with a low number of collocation points. ii) The error analysis confirms the spectral convergence of the method, as the error decreases exponentially with an increase in the number of basis functions N. iii) Comparative studies with existing methods, such as the variational iteration method, Legendre wavelets, and fractional Chebyshev pseudospectral methods, reveal that our SLSC technique achieves superior accuracy. iv) The method handles various continuous variable-order functions $\rho(t)$ effectively, and the numerical solutions consistently converge to the known integer-order solution as $\rho(t)\to 1$, validating the formulation's correctness. v) The successful application to a train motion control problem underscores the method's potential for solving real-world engineering systems modeled by VOF dynamics. In conclusion, the shifted Legendre spectral collocation method, empowered by the new VOFD operational matrix, presents a computationally efficient, theoretically sound, and numerically superior framework for tackling challenging VOFOC problems.

The success of this approach opens several promising avenues for future research: I) The methodology can be extended to solve VOFOC problems governed by PDEs in multiple spatial dimensions. II) Future work will focus on adapting the framework to handle more complex systems, such as fractional optimal control problems with time delays, state constraints, or hybrid variable-order fractional dynamics. III) The approach can be generalized to solve optimal control problems governed by variable-order fractional integro-differential equations. IV) While the FMINCON solver was effective, investigating specialized large-scale NLP solvers tailored to the structure of the resulting algebraic systems could further enhance computational efficiency for high-fidelity problems. V) Applying this numerical scheme to emerging fields such as bio-engineering, finance, and complex network control, where variable-order fractional models are increasingly being adopted, represents a significant future direction.

Declarations

Competing interests: The authors declare that they have no conflict of interest.
Authors' contributions: All authors have equally and significantly contributed to the contents of this manuscript.
Funding: The authors receive no funding for this research.
Availability of data and materials: There was no data utilized in the course of this investigation.

References

[1] Agrawal, O. P., Formulation of Euler-Lagrange equations for fractional variational problems. Journal of Mathematical Analysis and Applications, **272(1)** (2002), 368–379.
[2] Agrawal, O. P., A general formulation and solution scheme for fractional optimal control problems. Nonlinear Dynamics, **38(1-4)** (2004), 323–337.
[3] Agrawal, O. P., and Baleanu, D.. A Hamiltonian formulation and a direct numerical scheme for fractional optimal control problems. Journal of Vibration and Control, **13(9-10)**(2007), 1269–1281.
[4] Agrawal, O. P., Defterli, O., and Baleanu, D., Fractional optimal control problems with several state and control variables. Journal of Vibration and Control, **16(13)**(2010), 1967–1976.
[5] Ahmad, B., and Ntouyas, S. K., Existence of solutions for fractional differential inclusions with four-point nonlocal Riemann-Liouville type integral boundary conditions. Filomat, **27(6)**(2013), 1027–1036.

[6] Agrawal, O. P., A formulation and numerical scheme for fractional optimal control problems. Journal of Vibration and Control, **14(9-10)**(2008), 1291–1299.
[7] Alizadeh, A., and Effati, S., An iterative approach for solving fractional optimal control problems. Journal of Vibration and Control, **24(1)**(2018), 18–36.
[8] Almeida, R., Tavares, D., and Torres, D. F., The variable-order fractional calculus of variations . Springer, (2019), 27–29.
[9] Bahaa, G. M., Fractional optimal control problem for variable-order differential systems. Fractional Calculus and Applied Analysis, **20(6)**(2017), 1447–1470.
[10] Dehestani, H., Ordokhani, Y., and Razzaghi, M., Fractional-order Bessel wavelet functions for solving variable order fractional optimal control problems with estimation error. International Journal of Systems Science, **51(6)**(2020), 1032–1052.
[11] Guo, T. L., The necessary conditions of fractional optimal control in the sense of Caputo. Journal of Optimization Theory and Applications, **156(1)**(2013), 115–126.
[12] Gong, Q., Fahroo, F., and Ross, I. M., Spectral algorithm for pseudospectral methods in optimal control. Journal of Guidance, Control, and Dynamics, **31(3)**(2008), 460–471.
[13] Gong, Q., Ross, I. M., Kang, W., Fahroo, F., Connection between the covector maping theorem and convergence of pseudospectral methods for optimal control. Computational Optimization and Applications, **41**(2008), 307–335.
[14] Habibli, M., and Noori Skandari, M. H., Fractional Chebyshev pseudospectral method for fractional optimal control problems. Optimal Control Applications and Methods, **40(3)**(2019), 558–572.
[15] Heydari, M. H., Hooshmandasl, M. R., Ghaini, F. M., and Cattani, C. Wavelets method for solving fractional optimal control problems. Applied Mathematics and Computation, **286**(2016), 139–154.
[16] Heydari, M. H., A new direct method based on the Chebyshev cardinal functions for variable-order fractional optimal control problems. Journal of the Franklin Institute, **355(12)**(2018), 4970–4995.
[17] Heydari, M. H., and Avazzadeh, Z., A new wavelet method for variable-order fractional optimal control problems. Asian Journal of Control, **20(5)**(2018), 1804–1817.
[18] Lotfi, A., Dehghan, M., and Yousefi, S. A., A numerical technique for solving fractional optimal control problems. Computers and Mathematics with Applications,**62(3)** (2011), 1055–1067.
[19] Nemati, S., and Torres, D. F., Application of bernoulli polynomials for solving variable-order fractional optimal control-affine problems. Axioms, **9(4)**(2020), 114.
[20] Noori Skandari, M. H., Habibli, M., and Nazemi, A., A direct method based on the Clenshaw-Curtis formula for fractional optimal control problems. Mathematical Control and Related Fields, **10(1)**(2020), 171.
[21] Noori SKandari, M. H., and Ghaznavi, M., Chebyshev pseudo-spectral method for Bratu's problem. Iranian Journal of Science and Technology, Transactions A: Science, **41(4)**(2017), 913–921.
[22] Pedro, H. T. C., Kobayashi, M. H., Pereira, J. M. C., and Coimbra, C. F. M., Variable order modeling of diffusive-convective effects on the oscillatory flow past a sphere. Journal of Vibration and Control, **14(9-10)**(2008), 1659–1672.
[23] Pooseh, S., Almeida, R., and Torres, D. F., A numerical scheme to solve fractional optimal control problems. In Conference Papers in Science, (2013), Hindawi.
[24] Rabiei, K., Ordokhani, Y., and Babolian, E., The Boubaker polynomials and their application to solve fractional optimal control problems. Nonlinear Dynamics, **88(2)**(2017), 1013–1026.
[25] Vo, T. N., Razzaghi, M., Mihai, I., An approximate solution for variable-order fractional optimal control problem via Müntz-Legendre wavelets with an application in epidemiology. Mathematical Methods in the Applied Sciences, 46(13)(2023), 13645-13660.
[26] Sweilam, N. H., Al-Mekhlafi, S. M., and Al-Ajami, T. M., Optimal control of hybrid variable-order fractional coronavirus (2019-nCov) mathematical model; numerical treatments. Ecological Complexity, **49**(2022), 100983.
[27] Samko, S., Fractional integration and differentiation of variable order: an overview. Nonlinear Dynamics,**71(4)** (2013), 653–662.
[28] Shen J., Tang T. and Wang L. L., Spectral methods: Algorithms, analysis and applications, Springer, Berlin, (2011).
[29] Tajadodi, H., Efficient technique for solving variable order fractional optimal control problems. Alexandria Engineering Journal, **59(6)**(2020), 5179–5185.
[30] Zahra, W. K., and Hikal, M. M., Non standard finite difference method for solving variable order fractional optimal control problems. Journal of Vibration and Control, **23(6)**(2017), 948–958.
[31] Zelikin, M. I., Agrachev, A. A., Sachkov, Y., and Sachkov, Y. L., Control theory from the geometric viewpoint . Springer Science and Business Media, (2004).